ARMY RESEARCH LABORATORY

Measurement of Projectile Surface Temperature by Means of Its Infrared Radiation: A Preliminary Study

Keith P. Soencksen

ARL-MR-62 April 1993

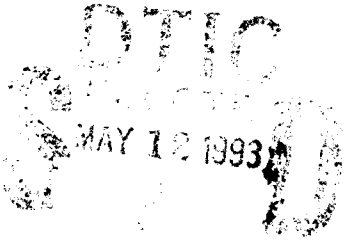

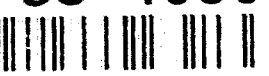

NOTICES

Destroy this report when it is no longer needed. DO NOT return it to the originator.

Additional copies of this report may be obtained from the National Technical Information Service, U.S. Department of Commerce, 5285 Port Royal Road, Springfield, VA 22161.

The findings of this report are not to be construed as an official Department of the Army position, unless so designated by other authorized documents.

The use of trade names or manufacturers' names in this report does not constitute indorsement of any commercial product.

REPORT DOCUMENTATION PAGE

Form Approved
OMB No 0704-0188

1. AGENCY USE ONLY (Leave blank)	2. REPORT DATE	3. REPORT TYPE AND DATES COVERED
	April 1993	Final, January 1992 - April 1992

4. TITLE AND SUBTITLE

MEASUREMENT OF PROJECTILE SURFACE TEMPERATURE BY MEANS OF ITS INFRARED RADIATION: A PRELIMINARY STUDY

5. FUNDING NUMBERS

PR: 1L161102AH43
WO: 61102A-00-001 AJ

6. AUTHOR(S)

KEITH P. SOENCKSEN

7. PERFORMING ORGANIZATION NAME(S) AND ADDRESS(ES)

U.S. Army Research Laboratory
ATTN: AMSRL-WT-PB
Aberdeen Proving Ground, MD 21005-5066

8. PERFORMING ORGANIZATION REPORT NUMBER

9. SPONSORING/MONITORING AGENCY NAME(S) AND ADDRESS(ES)

U.S. Army Research Laboratory
ATTN: AMSRL-OP-CI-B (Tech Lib)
Aberdeen Proving Ground, Maryland 21005-5066

10. SPONSORING/MONITORING AGENCY REPORT NUMBER

ARL-MR-62

11. SUPPLEMENTARY NOTES

12a. DISTRIBUTION/AVAILABILITY STATEMENT

Approved for public release; distribution is unlimited.

12b. DISTRIBUTION CODE

13. ABSTRACT *(Maximum 200 words)*

The current work is a preliminary study to planned direct measurement of the infrared emissions of a projectile in flight, from which surface temperature will be estimated. If the planned experiment is to be meaningful, the projectile surface temperature must be high enough such that the incident infrared radiation is significant enough to be measured by the detectors. In this report, detector threshold is calculated and compared to the computed infrared radiation reaching the detector from an M735 projectile nosecone at a distance from the muzzle of 225 meters. In the wavelength band 2.0 - 2.5 mu, the results predict that the detector will not be able to see the projectile emissions, and in the wavelength band 3.5 - 4.0 mu, the results show probable detection of most of the projectile only if the flow is turbulent.

14. SUBJECT TERMS	15. NUMBER OF PAGES
Infrared Radiation Projectiles Surface Temperature	28
	16. PRICE CODE

17. SECURITY CLASSIFICATION OF REPORT	18. SECURITY CLASSIFICATION OF THIS PAGE	19. SECURITY CLASSIFICATION OF ABSTRACT	20. LIMITATION OF ABSTRACT
UNCLASSIFIED	UNCLASSIFIED	UNCLASSIFIED	UL

INTENTIONALLY LEFT BLANK.

Acknowledgements

The author would like to extend his sincere appreciation to those individuals instrumental in this study and report.

First, Dr. George Thomson has been the author's advisor throughout this preliminary study. Dr. Thomson provided necessary guidance and assistance throughout.

Secondly, Mr. Bernard Guidos has performed the computational prediction of the experimental conditions discussed in the results. This involved the use of a parabolized Navier-Stokes (PNS) computational code on a Cray X-MP/48 supercomputer located at the BRL. Mr. Guidos is credited with the computational predictions shown in Figures 10 and 11.

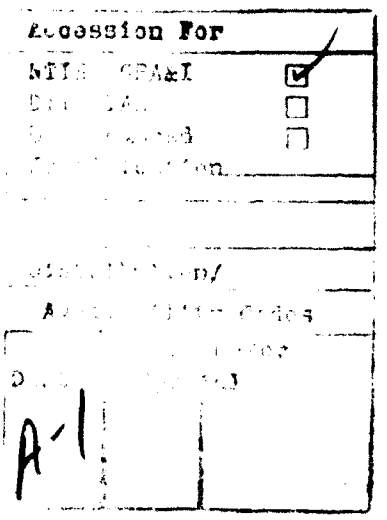

INTENTIONALLY LEFT BLANK.

TABLE OF CONTENTS

INTENTIONALLY LEFT BLANK.

LIST OF FIGURES

LIST OF TABLES

INTENTIONALLY LEFT BLANK.

1. INTRODUCTION

As flight velocities increase, the study of projectile heat transfer is of growing interest to the Army.

Of considerable concern in ballistic heat transfer is projectile surface temperature. Temperature is used, for example, as a design tool, for determination of appropriate projectile materials and shapes. While there are a significant number of numerical codes which predict projectile surface temperatures for a variety of conditions, relatively little experimental data has been produced for the purpose of verifying these numerical predictions [1]. Lowe [2] has published data from an experiment conducted in 1951, in which the surface temperatures of 30-caliber projectiles were measured by comparing the infrared radiation emitted by the bullets with the radiation from a hot background of known and variable temperature. The data from this experiment are very limited. In addition, Lowe's method requires repeated shots at the same flight conditions to determine surface temperature.

The current work has been done as a preliminary study to planned work which will result in the experimental determination of projectile surface temperatures through the measurement of projectile infrared emissions.

The infrared power emitted from an aerodynamically heated projectile, and thus the detector's current output recorded, is largely dependent upon the projectile's temperature [3]. However, because of the natural physical limitations associated with electronic noise, infrared detectors cannot detect an infinitely small signal. If the planned experiment is to be meaningful, the projectile surface temperature must be high enough such that the incident infrared radiation is significant enough to be measured by the given detectors.

It is the purpose of this study to determine whether or not the expected infrared radiation will be significant enough to be measureable, given the detector specifications. This will be done by modeling both detector response and projectile emissions.

2. ANALYSIS

The study will proceed as follows. First, we will use infrared detection theory to determine the minimum amount of radiant power in Watts which will be measureable, the *detector threshold*, given the specifications of one of the indium-antimonide detectors to be used. Next, we will calculate the amount of infrared radiant power leaving the projectile surface as a result of its temperature. The analysis will then calculate that fraction of the total radiation emitted which actually reaches the detectors and falls within special wavelength sensitivity bands set by filters.

Several assumptions are made. First, we will assume that at any given instant, all the projectile surface area which falls within the field of view of the detectors (described below) is at a constant temperature. If this assumption is not made, the future experimental study will be useless, since the detectors will only measure some type of average of perhaps several different temperatures which exist on different parts of the surface. In order to make this assumption accurate, the field of view of the detectors is set such that only a very small

amount of projectile surface area is visible. Next, zero angle of attack is assumed. Lastly, we assume that the projectile is the only source of radiation which reaches the detectors.

2.1 Detector Threshold Power A group of three commercially available indium-antimonide infrared detectors will be placed in a specially designed housing which exposes part of the detector surface to external radiation, but which shields this surface from background radiation and noise. The detectors are sensitive to wavelengths in the infrared region. An approximate view of this experimental apparatus is shown in Figure 1. The width of the aperture shown at the top of the detector housing can be adjusted, thus allowing control of both the amount and direction of incoming radiation. The "field of view" can be defined as the space above the detector housing that is visible to the detectors. This field of view is shown (from an axial direction) as the shaded region in Figures 2 and 3. As shown in Figure 2, the projectile penetrates this field of view, thus exposing approximately 180 degrees of the projectile's cylindrical surface over the width of the field of view (shown in Figure 3). The width of the field of view is dependent upon both the width of the aperture and the height of the projectile above the detectors, as shown in Figure 3. The infrared radiant power that is emitted from the projectile and is incident on the detectors will be electronically converted to a current, then recorded and output.

The author-defined term, *detector threshold*, will be determined from expressions of figures of merit commonly used to compare the performance of one detector to another. A basic figure of merit is *current responsivity*, R_i, defined as the ratio of current output (i_s, Amperes) to radiant power (ϕ_e, Watts):

$$R_i(\lambda) = \frac{i_s}{\phi_e(\lambda)}$$

where λ indicates the wavelength of the incident radiation [4]. The detectors have been tested by the manufacturer, who has supplied both peak responsivity and spectral responsivity (relative to peak responsivity). A plot of the spectral responsivity for the detector under analysis is shown in Figure 4.

Electronic rms *noise*, (i_{rms}, Amps/$\sqrt{Hz}$), is inherently associated with the detector circuit. Note that the units associated with this definition of noise show a frequency dependence. The reason for this is that the noise will be inversely proportional to the square root of the frequency bandwidth of the output device's filter [5,6]. The above definition of rms noise implicitly assumes that the device connected to the detector circuit output (e.g., a spectrum analyzer) utilizes a filter which rejects all frequencies except those in a 1 Hz bandwidth. The effect of a larger bandwidth is to allow more noise into the circuit. Hence, if the measurement device to be used employs a filter with a bandwidth larger than 1 Hz, then we must account for this by multiplying the rms noise in Amps by the square root of this bandwidth in Hz to obtain the total actual noise [5]. For example, a measurement device which has a filter with a 10 kHz bandwidth, will increase the noise by a factor of 100.

The *noise equivalent power* (NEP) of a detector is defined as the incident power which will produce a signal output equal to the rms noise output [4,7]. Since the current signal output is

$$i_s = R_i \phi_e$$

the signal-to-noise ratio can be expressed as

$$S/N = \frac{R_i \phi_e}{i_{rms}}$$

The incident radiant power, ϕ_e, becomes the NEP when the signal-to-noise ratio is 1. Thus,

$$NEP = \frac{i_{rms}}{R_i} \tag{1}$$

where, as above, the units of rms noise are (Amps/$\sqrt{Hz}$) and the units of responsivity are Amps/Watt.

Equation 1 then, represents the minimum radiant power (in Watts) which is detectable, the *detector threshold*, for the given circuit. However, the NEP will vary, since the detector's responsivity varies with the wavelength of incident radiation (Figure 4). For simplicity, we will average the responsivity over the range of wavelengths of interest for the detectors. As stated earlier, a filter will be placed on each detector, limiting its response to only radiation within a small wavelength band. This is in part due to the fact that infrared radiation does not transmit through the atmosphere without significant attenuation at some wavelengths [1,8]. Hence the filters will be used such that all wavelengths which are accepted by each filter will be transmitted with little or no attenuation to the detector. The bandwidths of these filters will each be approximately 0.5μ, but each filter will be centered at a different infrared wavelength. In the analysis, the responsivity used in Equation 1 will be the average over a particular wavelength band of interest. Noise on the other hand, will be constant with wavelength [5].

2.2 Projectile Radiant Power In this section, we calculate the amount of radiant power emitted by the heated projectile. Next, that fraction of radiant power which leaves the projectile *and* reaches the detectors, will be determined.

In the planned experiment, an aerodynamically heated projectile will fly above the special infrared detector housing. In doing so, part of the projectile will be within the field of view of the detectors as shown schematically in Figures 2 and 3.

For now, we will consider a single detector at a single instant in time and consider that some part of the projectile cylinder is within the detector's field of view. We are only interested in the infrared radiation emitted from the portion of the projectile which is within the detector's field of view at the given instant.

We will assume that both the projectile surface and the detector behave as blackbodies, that is, both surfaces absorb all incident radiation and are also perfect radiators. Planck's Law describes the spectral distribution of radiation from such a surface as [7]

$$W_\lambda = \frac{c_1}{\lambda^5} \frac{1}{e^{c_2/\lambda T} - 1} \tag{2}$$

where,

W_λ=spectral radiant emittance, $W cm^{-2} \mu^{-1}$

λ=wavelength, μ

T=absolute temperature, $^\circ K$
c_1=first radiation constant=$3.7415 \times 10^4 W cm^{-2} \mu^4$
c_2=second radiation constant=$1.43879 \times 10^4 \mu K$

A plot of this spectral distribution is shown in Figure 5. Notice from this plot that the total radiant emittance (proportional to the area under the curves) increases rapidly with temperature. Also, the curves never cross one another, hence, a higher temperature will always give higher spectral emittance. If we integrate this spectral distribution over all wavelengths, we obtain

$$\int_0^\infty W_\lambda d\lambda = W_{0-\infty} = \sigma T^4$$

where σ is a constant.

The given detectors are sensitive to a small band of wavelengths set by detectors. These bands, for the calculation of the preceding section, are $2.0\mu - 2.5\mu$ and $3.5\mu - 4.0\mu$, since these bands are transmitted through the atmosphere with little or no attenuation. Hence we will be interested in the amount of energy radiated *only* from the part of the projectile surface within the field of view and *only* within these wavelength bands. The radiant energy emitted between any two wavelengths λ_1 and λ_2 can be obtained by [3]:

$$W_{\lambda_1-\lambda_2} = \int_{\lambda_1}^{\lambda_2} W_\lambda d\lambda \tag{3}$$

We have obtained an expression (Equation 3) for the radiant emittance per square centimeter in the wavelength band of detector sensitivity. We now need an expression for the power (Watts) which leaves the surface area of interest and arrives at the detector. If we multiply Equation 3 by the surface area of the source of the energy (surface area of the projectile that is within the detector's field of view) then we obtain the total amount of power leaving this surface per unit time (in Watts). However, since this energy is emitted in all directions, only a small fraction of it will be incident on the detector. Thus, it is appropriate to represent the amount of radiant emittance leaving this portion of the projectile's surface and arriving at the detector by [3]:

$$W_{\lambda_1-\lambda_2} A_{proj} F_{proj-det} \tag{4}$$

where,

A_{proj}=area of projectile within detector field of view
$F_{proj-det}$=fraction of energy leaving A_{proj} which reaches detector

In Equation 4 above, $F_{proj-det}$ is directly related to the geometric orientation between the projectile surface and the detector surface. This orientation is shown in Figure 6 for a cylindrical section of the projectile. More specifically, $F_{proj-det}$ is related to the angles formed between a line connecting the two surfaces and the normal to each surface. These angles are shown in Figure 6 as ϕ_1 and ϕ_2. From the figure, we notice that ϕ_1 and ϕ_2 change continuously as we move around the cylindrical surface of the projectile, hence, we must integrate differential areas, dA_{proj}. A detailed derivation [3] shows that:

$$A_{proj} F_{proj-det} = \int_{A_{det}} \int_{A_{proj}} \cos\phi_1 \cos\phi_2 \frac{dA_{proj} dA_{det}}{\pi r^2} \tag{5}$$

where r is the distance between the differential element and the detector. Then, on combining Equations 3, 4 and 5, we get:

$$W_{\lambda_1-\lambda_2} A_{proj} F_{proj-det} = \left(\int_{\lambda_1}^{\lambda_2} W_\lambda d\lambda \right) \int_{A_{det}} \int_{A_{proj}} \cos\phi_1 \cos\phi_2 \frac{dA_{proj} dA_{det}}{\pi r^2} \qquad (6)$$

The detectors to be used are square. However, in the planned experimental setup, most of the detector surface area will be covered so as to limit the detector's field of view width. Thus the detector's *exposed* area will be approximately rectangular in shape, with a width of 0.0508 centimeters, and a length approximately equal to the detector diagonal, L (see Figure 7). Since the area of the projectile is much greater than that of the exposed part of the detector, we will consider the exposed detector area to be differential in size. This means that we can eliminate the integral over A_{det}. Then, Equation 6 becomes,

$$W_{\lambda_1-\lambda_2} A_{proj} F_{proj-det} = (0.0508L) \left(\int_{\lambda_1}^{\lambda_2} W_\lambda d\lambda \right) \int_{A_{proj}} \cos\phi_1 \cos\phi_2 \frac{dA_{proj}}{\pi r^2} \qquad (7)$$

An expression for the surface area, dA_{proj}, will depend on which particular portion of the projectile is within the detector's field of view at the given instant. An infinite number of possibilities exist, however these can be divided into three broad categories. The area of the projectile within the detector's field of view can be part of the projectile's

- nosecone section
- cylindrical body section
- finned tail section

The reason for the above categorization will become evident below.

If a portion of the cylindrical body section of the projectile is above the detector, then the surface area which is visible to the detector is approximately the lower semi-cylindrical surface over a length equal to the field of view width at the projectile (see Figure 6). The field of view width at the projectile is approximately

$$\text{width} = 2h \tan\beta$$

where h is the height of the projectile above the detector and β is the aperture half angle (Figure 3). The width of each differential element (from Figure 6) is $R\,d\theta$, where R is the projectile radius. Hence,

$$dA_{proj} = 2hR \tan\beta\, d\theta$$

From this, Equation 7 becomes

$$W_{\lambda_1-\lambda_2} A_{proj} F_{proj-det} = (0.0508L) \left(\int_{\lambda_1}^{\lambda_2} W_\lambda d\lambda \right) \int_0^{\pi} \cos\phi_1 \cos\phi_2 \tan\beta \frac{2hR\, d\theta}{\pi r^2} \qquad (8)$$

where, from geometric analysis,

$$\phi_1 = \tan^{-1} \left[\frac{R\cos\theta + y}{h - R\sin\theta} \right]$$

$$\phi_2 = \tan^{-1}\left[\frac{R\cos\theta + y}{h - R\sin\theta}\right] + \frac{\pi}{2} - \theta$$

In the equations for ϕ_1 and ϕ_2, y is the distance between the center of the detector and the line of flight at the detector level (Figure 6).

If a portion of the conical nosecone of the projectile is above the detector, then the surface area which is visible to the detector is approximately the lower semi-conical surface over a length equal to the field of view width at the projectile (see Figure 8). This complicates the analysis slightly since several geometric variables are no longer constant over the width of the field of view. That is, ϕ_1, ϕ_2, r and R all become functions of x (Figure 8). The effect of this is seen in forming an expression for dA_{proj} as follows. First, let us add the non-orthogonal coordinate w to the standard xyz coordinate system in such a way that w is parallel to the projectile surface along the nosecone. This is shown in Figure 8. We have,

$$dA_{proj} = R\, d\theta\, dw \tag{9}$$

Hence we see that we will need to integrate differential areas first along the nosecone (in w), and then circumferentially (in θ). Next,

$$R = x\tan\alpha \tag{10}$$

where α is the nosecone angle. Finally,

$$dw = \frac{dx}{\cos\alpha} \tag{11}$$

Now, combining Equations 9, 10 and 11, we get,

$$dA_{proj} = x\frac{\tan\alpha}{\cos\alpha}\, dx\, d\theta \tag{12}$$

Also, the angle formed between the line connecting the two surfaces (detector and projectile) and the normal to the projectile surface has now changed. It has now become the combination of ϕ_2 and α, as shown in Figure 8. Given all this, we obtain the equivalent to Equation 8 for a section of the nosecone as:

$$W_{\lambda_1-\lambda_2} A_{proj} F_{proj-det} = (0.0508L)\tan\alpha \left(\int_{\lambda_1}^{\lambda_2} W_\lambda d\lambda\right) \int_0^{\pi}\int_{x_1}^{x_2} \cos\phi_1 \cos\phi_2 \frac{x}{\pi r^2}\, dx\, d\theta \tag{13}$$

For simplicity, we assume that the field of view width is the same as that used in the analysis of the cylindrical section above. This assumption leads to the value of the second integration limit in x, once the initial point, x_1, is chosen on the nosecone. Equation 13 then becomes,

$$W_{\lambda_1-\lambda_2} A_{proj} F_{proj-det} = (0.0508L)\tan\alpha \left(\int_{\lambda_1}^{\lambda_2} W_\lambda d\lambda\right) \int_0^{\pi}\int_{x_1}^{x_1+2h\tan\beta} \cos\phi_1 \cos\phi_2 \frac{x}{\pi r^2}\, dx\, d\theta \tag{14}$$

In Equations 13 and 14 above, ϕ_1 and ϕ_2 are defined exactly as before.

If a portion of the projectile's tail section is above the detector, although the detector will be receiving infrared radiation, prediction of surface temperature is impossible. This is because of the assumption made earlier that at any given instant, all the projectile surface

area which falls within the field of view of the detectors is at a constant temperature. In the case of a finned tail section, the fin leading edges will be at a temperature which is vastly different from that of the fin roots, for example. When the tail section is within the field of view of the detectors, the detectors will likely see many different portions and combinations of the fins and projectile cylinder, with each portion being at a different temperature. Hence, the planned experiment will not attempt to measure the surface temperature in this region. It is noted however that the possibility exists for infrared surface temperature measurement in the case of a conical flared afterbody.

3. RESULTS

The measurement equipment to be used in the planned experimental work has a maximum noise frequency bandwidth of approximately 1 MHz [1]. Hence, the noise associated with each detector's circuit will be multiplied by 1000. Also, as recommended by the manufacturer, an additional "safety factor" of 10 will be used, thus making the noise multiplication factor 10,000. This important step will insure a conservative estimate of the minimum detectable power.

As stated previously, filters will be placed on each detector such that all wavelengths which are accepted by each filter will be transmitted with little or no atmospheric attenuation to the detector. Data indicate [8] that infrared radiation is transmitted with nearly zero distortion in the wavelength bands 2.0μ-2.5μ and 3.5μ-4.0μ. Hence, these wavelength bands will be considered for use in each detector's filter.

Calculation of the detector threshold is performed in Table 1 for a single representative detector, since the other detectors to be used have not yet been purchased. The calculation is performed using the detector test data as supplied by the manufacturer and listed in Table 2.

Now that we have calculated the minimum amount of infrared radiated power which the detector will accept, we must calculate how much power will actually leave the projectile's surface (within the detector field of view) and reach the detector. This is done using Equation 8 for a cylindrical portion of the projectile, and using Equation 14 for a section of the projectile's conical nose. The projectile used for the current calculations is the M735 kinetic energy, fin-stabilized, 105mm round. At present, this round is one of several likely candidates for use in the future experimental work [1].

Equations 8 and 14 are solved using a code written by the author. The first calculation is the amount of infrared radiation within the wavelength band set by the detector's filter which leaves the portion of the projectile that is within the detector field of view:

$$\int_{\lambda_1}^{\lambda_2} W_\lambda d\lambda$$

This quantity is obtained numerically by direct calculation of Equation 2 between the above intervals using several different sizes of wavelength increments to obtain a final answer of accuracy $O(h^6)$, where h is the size of the smallest increment used [10]. This method of numerical integration, called Romberg integration, is an improvement of the trapezoidal

rule.

Next, the quantities α, R and L are known, and values for h and β are assumed. These quantities are shown in Table 3. Using this information, the code described above calculates ϕ_1, ϕ_2, and r for any given θ. The integrations are performed again using Romberg integration.

The algorithm used in the code is as follows. A projectile surface temperature is assumed for a given slice of projectile within the detector's field of view. Using this temperature, the code calculates the amount of radiant power incident upon the detector, as described above. This amount of radiant power (in Watts) is compared to the detector threshold. If it is less than the detector threshold, then the detector will not be able to see that particular section of projectile at that particular temperature. Consequently, the temperature is increased by a small increment and the process is repeated. The temperature is increased until the power received at the detector is *greater* than the detector threshold. This temperature is the *minimum temperature* of the particular section of projectile being analyzed, in order for the detector to see it.

Since the nose will be hotter than the cylinder, it may seem that the area of greatest concern relative to achieving the detector threshold would be the projectile cylinder. In fact, the opposite is true for the following reason. While it is true that a section of a higher temperature will emit more *total* infrared energy than an equivalent section at a lower temperature, what matters is the energy emitted *per unit area.* As we approach the nose tip the energy per unit area increases (since temperature increases), but surface area approaches zero. The net effect of this trade-off is that the *total* energy approaches zero.

This is shown in Figure 9. This figure shows *Detector Threshold Temperature* (minimum temperature for detection) as a function of length down the nosecone for both wavelength bands of interest. First, note that the effect of less and less surface area (approaching the nosetip) is to require a higher temperature for detection. Obviously, a detector which accepts wavelengths in the band 3.5μ-4.0μ requires a much lower temperature than a detector which is sensitive to the band 2.0μ-2.5μ. This is for two reasons. First, referring to Figure 5, we see that in the higher band of wavelengths, the spectral radiant emittance is greater. Secondly, referring to Figure 4, we note that the responsivity of the detector is greater in the higher wavelength band.

In order to achieve meaningful results, this study also pursued the computational prediction of the anticipated experimental conditions. In the planned experiment, the special detector housing will be placed approximately 225 meters downrange of the muzzle. Hence we desire a computational prediction of the nosecone surface temperature of the M735 projectile at a range of 225 meters when launched at normal service velocity (M=4.36). The computational approach performed by Guidos [10] first utilizes a parabolized Navier-Stokes technique to compute surface heat transfer rates, and then computes the in flight thermal response using a finite-volume heat conduction technique. Results from this computation are shown in Figures 10 and 11 together with the results of the above calculations of detector threshold on the nose. Figure 10 shows the predicted surface temperature versus projectile length for fully laminar flow, while Figure 11 shows the same quantity for fully turbulent flow.

4. CONCLUSIONS

In this study, we have calculated the detector threshold for a given infrared detector and compared it to the calculated amount of radiation which reaches the detector from an M735 projectile nosecone. From this comparison the detector threshold temperature has been determined for these conditions. Finally, the detector threshold temperature has been compared to the surface temperatures which are computationally predicted 225 meters from the gun, for a launch velocity of M=4.36.

From Figure 9, we note that a filter with a wavelength band of 3.5μ-4.0μ is preferred over that of 2.0μ-2.5μ, since a much lower detector threshold temperature results.

Furthermore, from Figures 10 and 11, we note that the detector threshold temperatures required by the wavelength band 2.0μ-2.5μ will most likely never be realized even for fully turbulent flow. By similar comparison in the wavelength band 3.5μ-4.0μ, detector threshold temperature will probably only be reached if the flow is fully turbulent. Even in this case, the threshold may not be reached very close to the nose tip. In this wavelength band then, detector threshold temperature should be realized approximately 1-2 cm downstream of the nose tip, and thereafter, assuming turbulent flow.

Results of the Guidos temperature computations shown in Figures 10 and 11 are encouraging. These results predict that the highest temperature in the nose region will occur at the nose tip, and that the temperature here will be significantly higher than that on the cylindrical section of the projectile. Thus it is predicted that two hot regions will exist on the projectile (the nose and the tail). This is desireable for the proper operation of the infrared instrumentation.

Two recommendations are evident which will increase the possibility of success in the planned experiment. First, use a measurement device with a smaller noise frequency bandwidth. This will allow less noise to enter the circuit, and thereby increase the sensitivity of the detector (that is, the detector threshold would decrease). Secondly, utilize a boundary layer trip device as close to the projectile nose tip as possible to insure turbulent flow. Reasons for this are evident from the previous discussion, and are discussed in Reference 10 by Guidos.

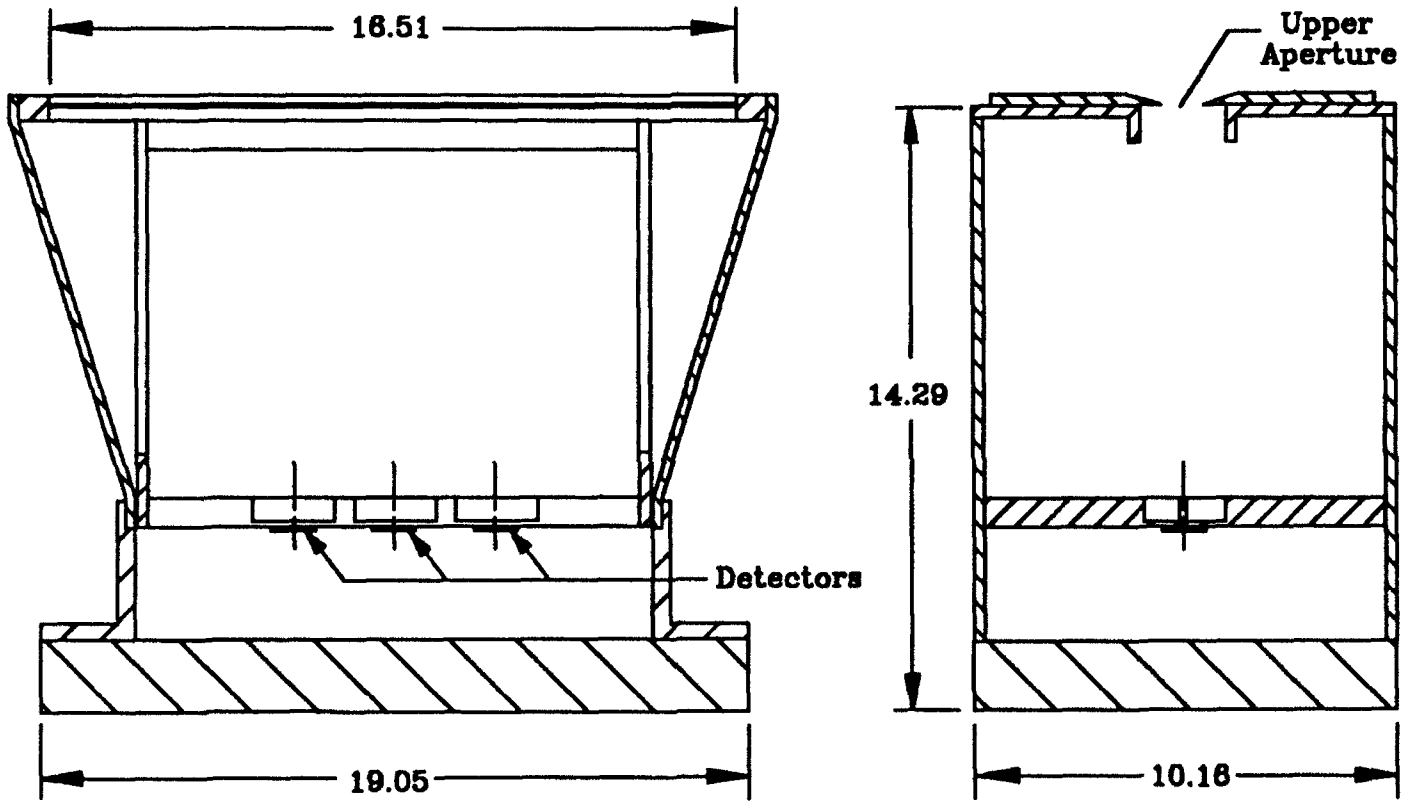

Figure 1. Infrared Detector Housing

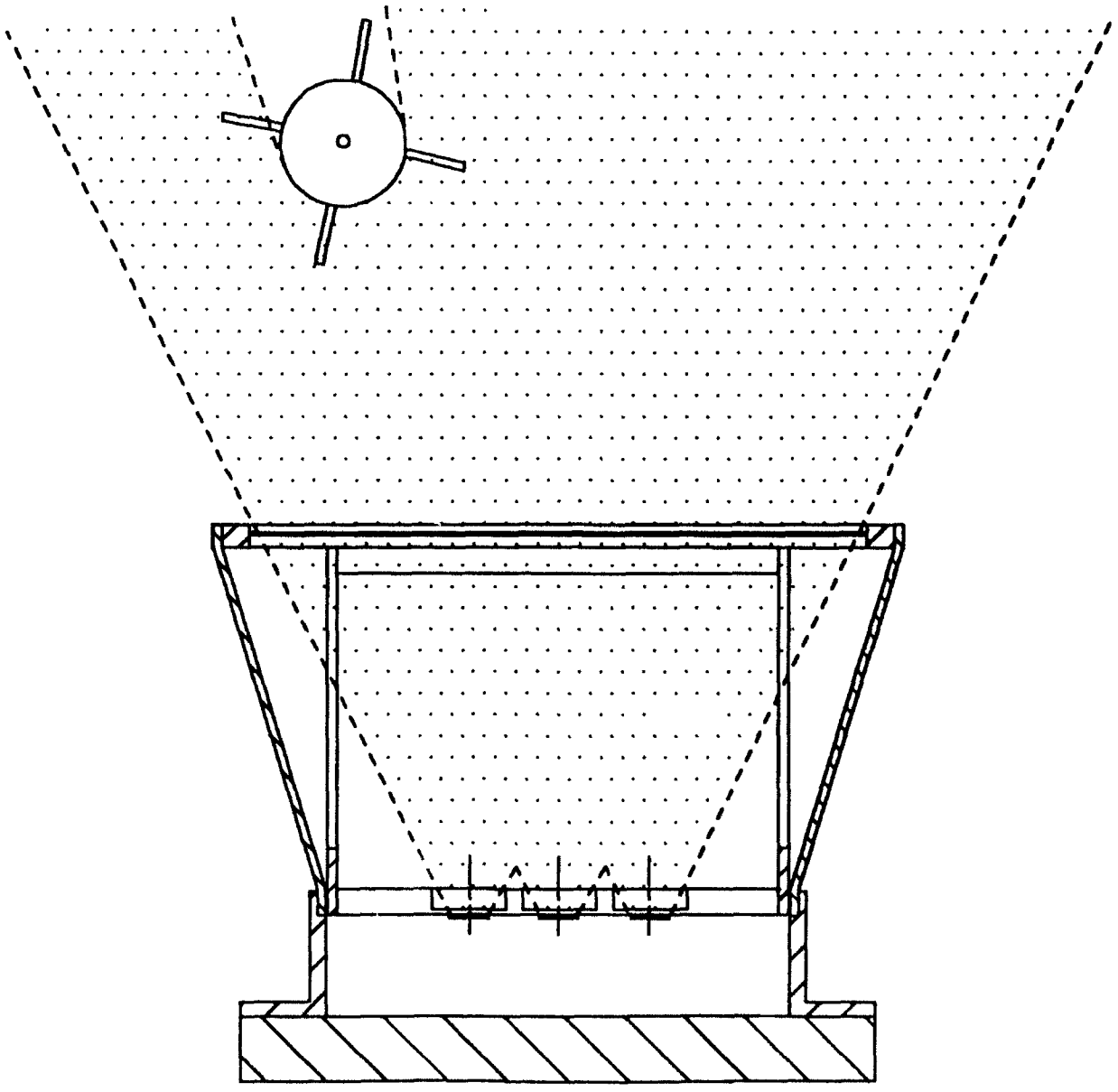

Figure 2. Housing and Detector Field of View, Front View

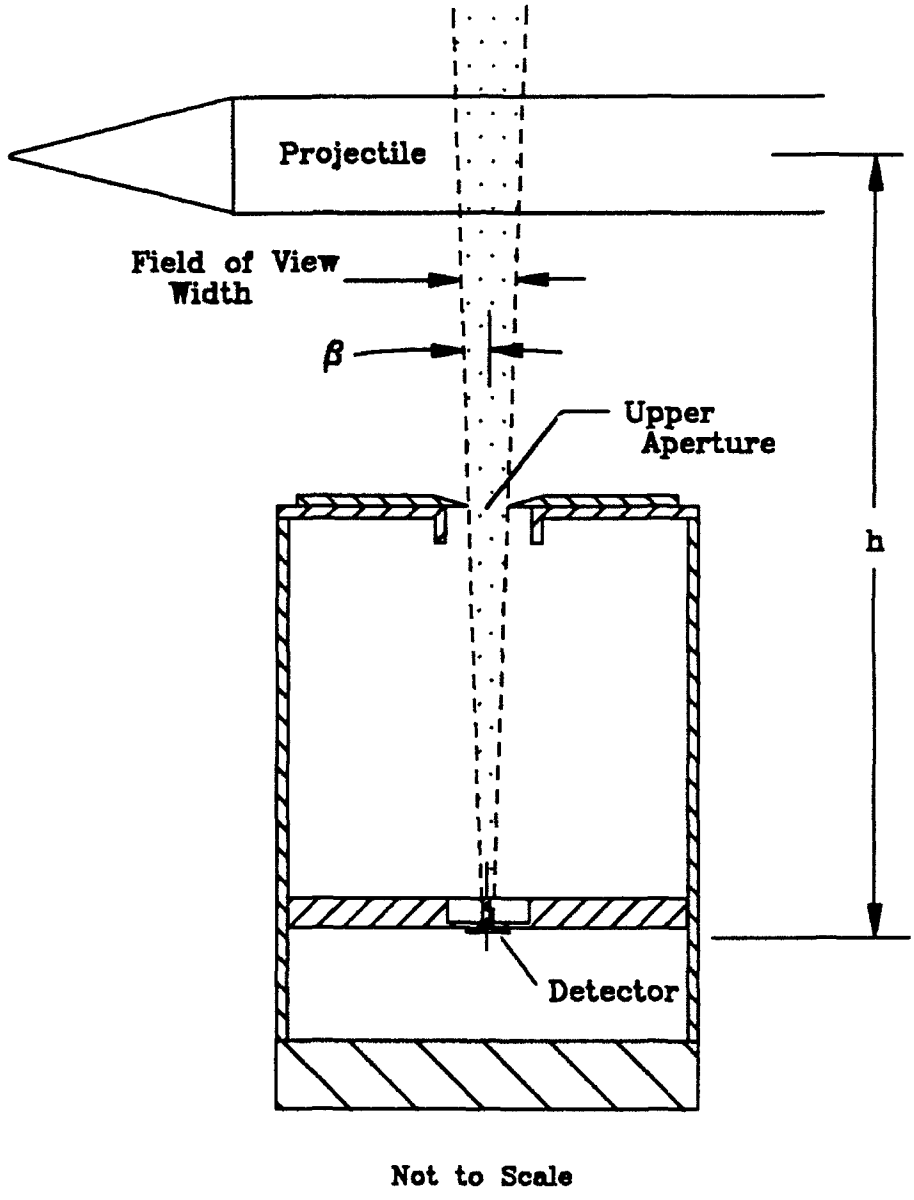

Figure 3. Housing and Detector Field of View, Side View

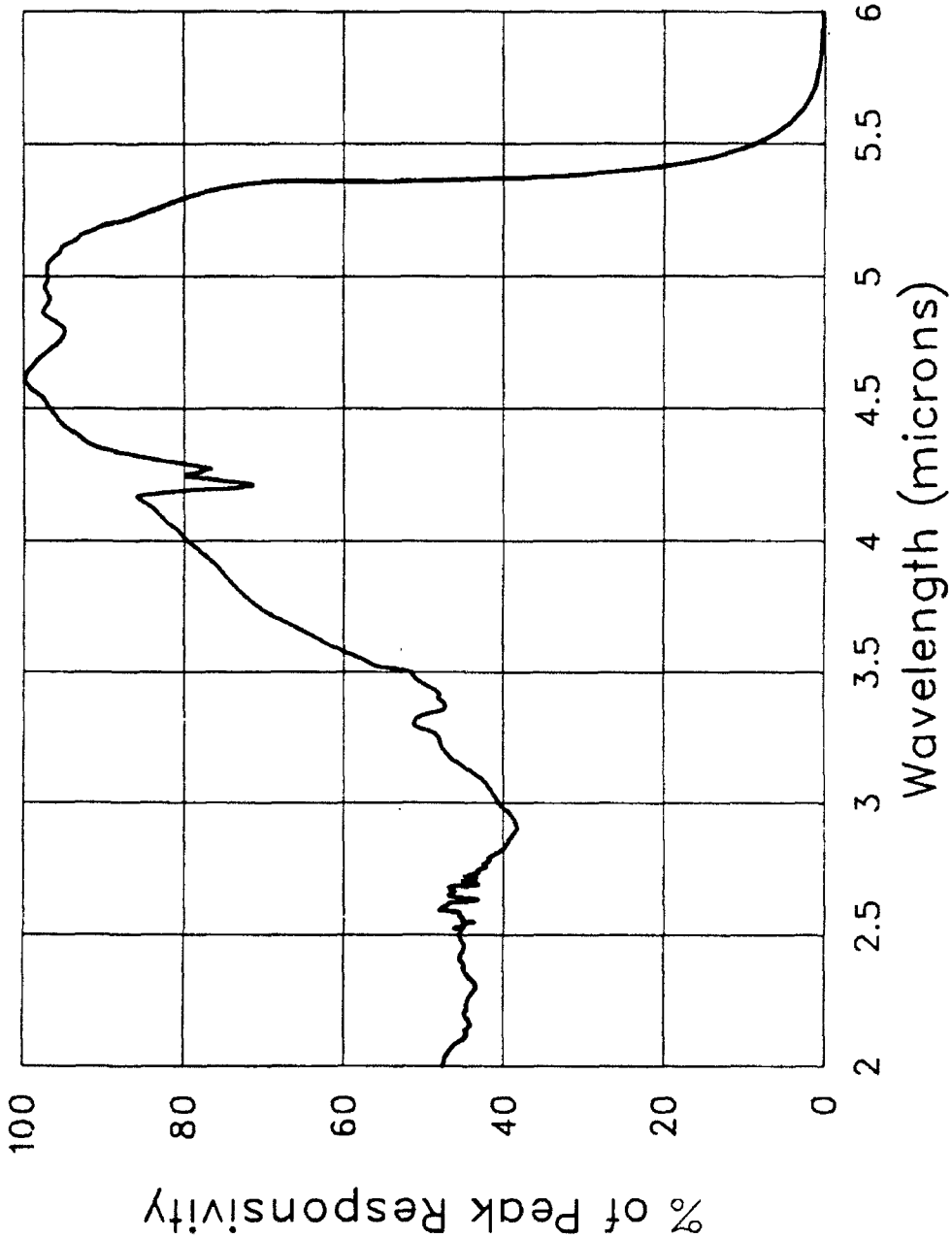

Figure 4. Spectral Responsivity, EG and G Judson Indium-Antimonide Detector

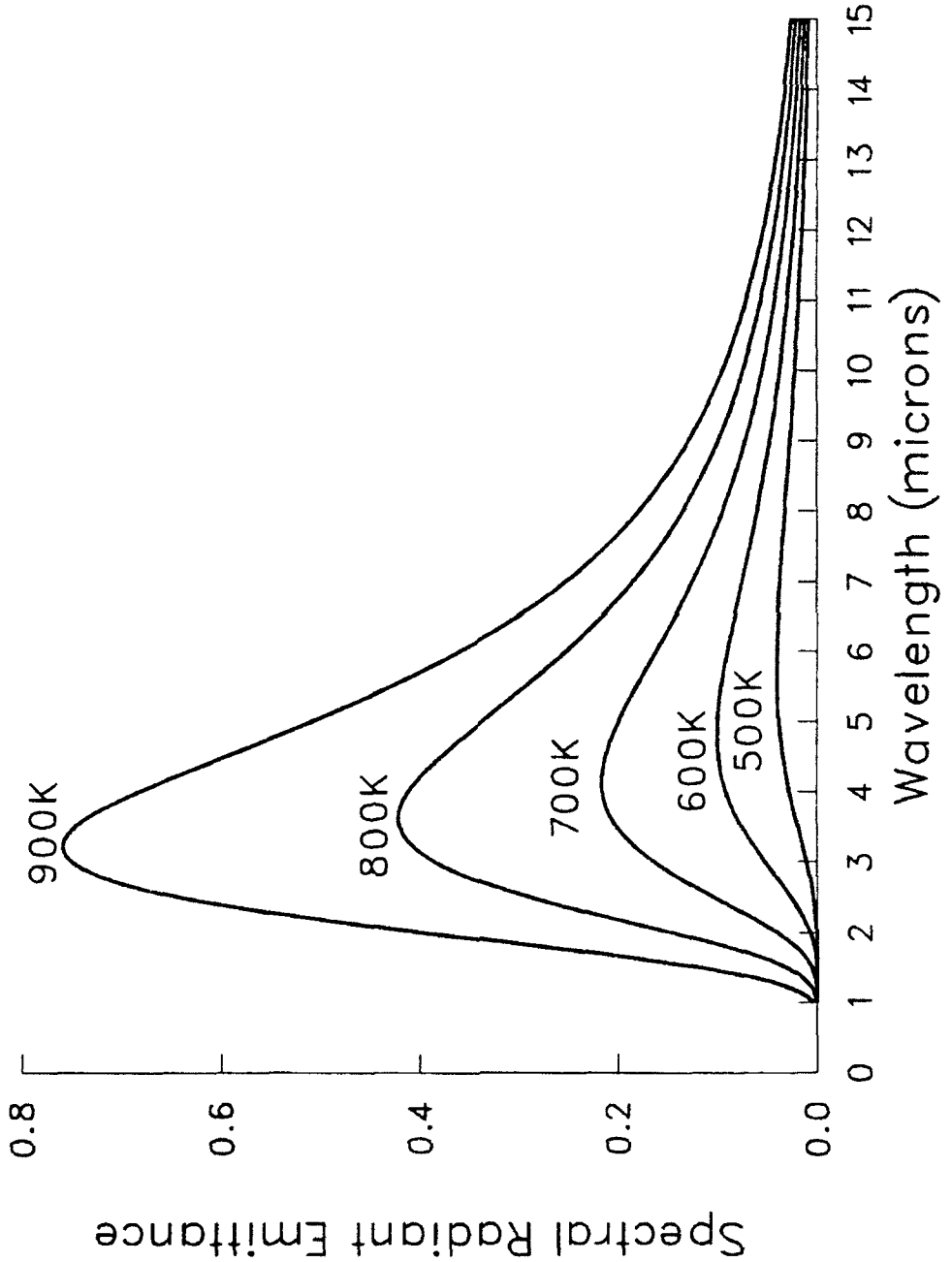

Figure 5. Planck's Law

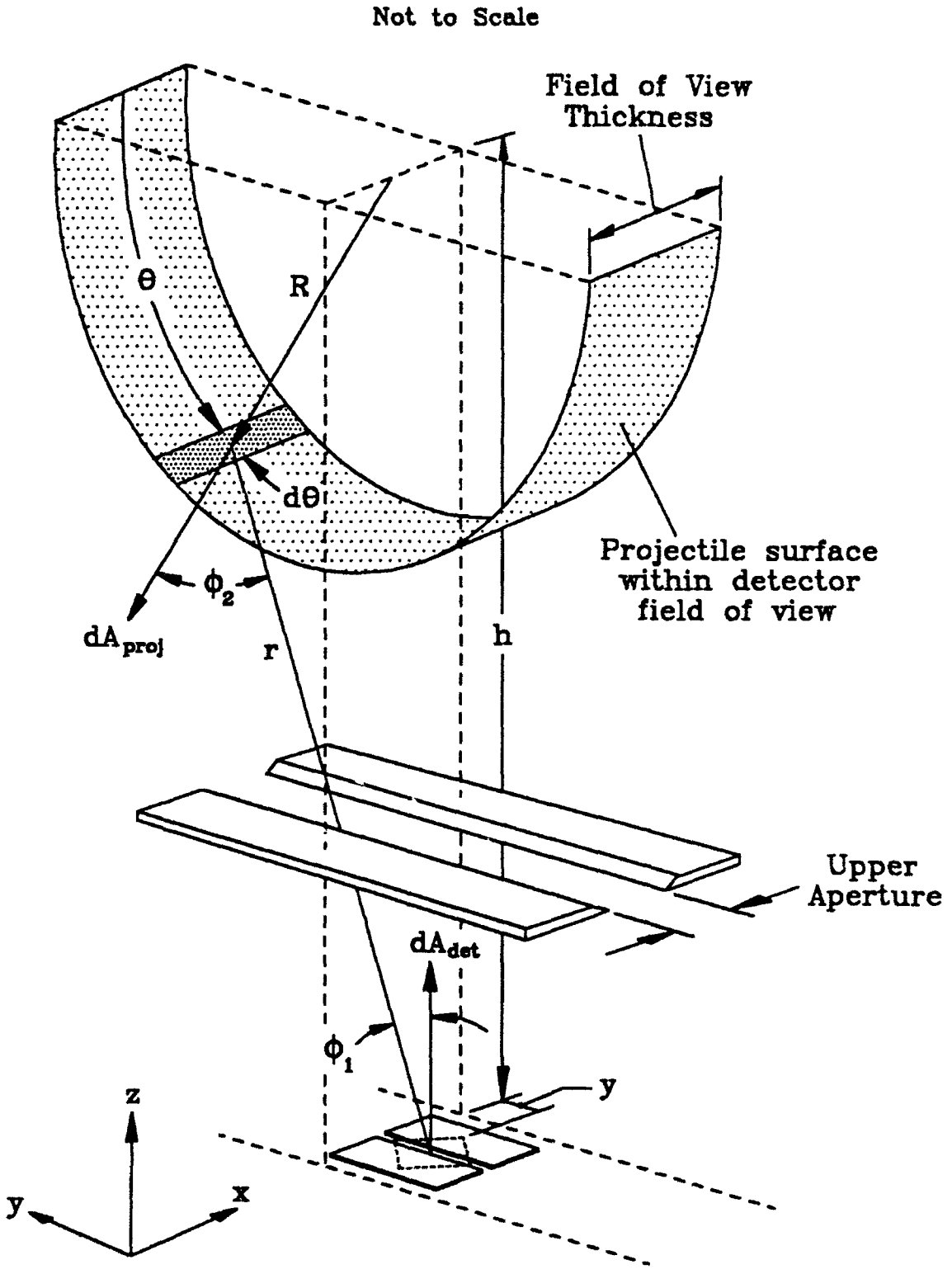

Figure 6. Experimental Configuration for a Portion of Projectile Cylinder

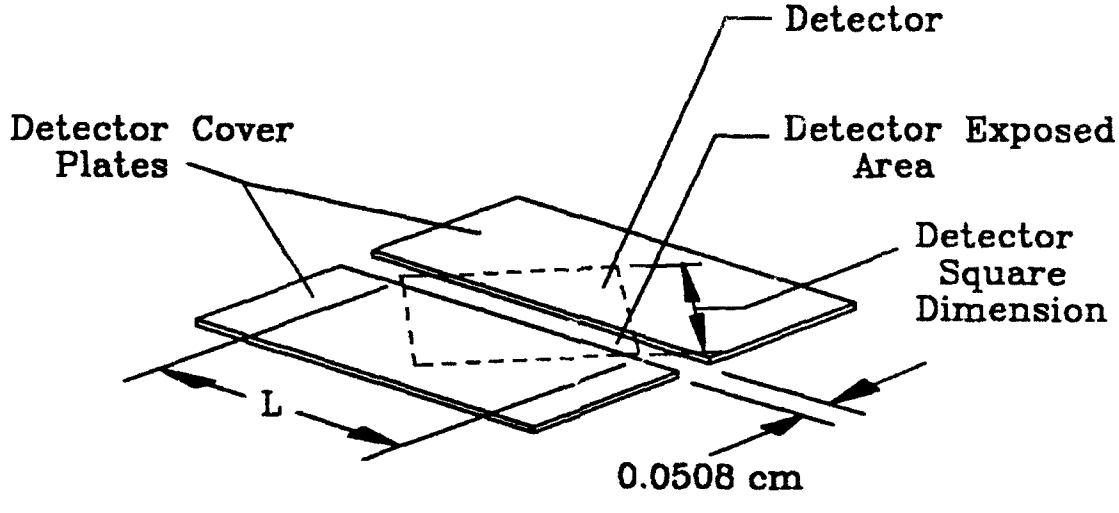

Figure 7. Experimental Setup of Detector

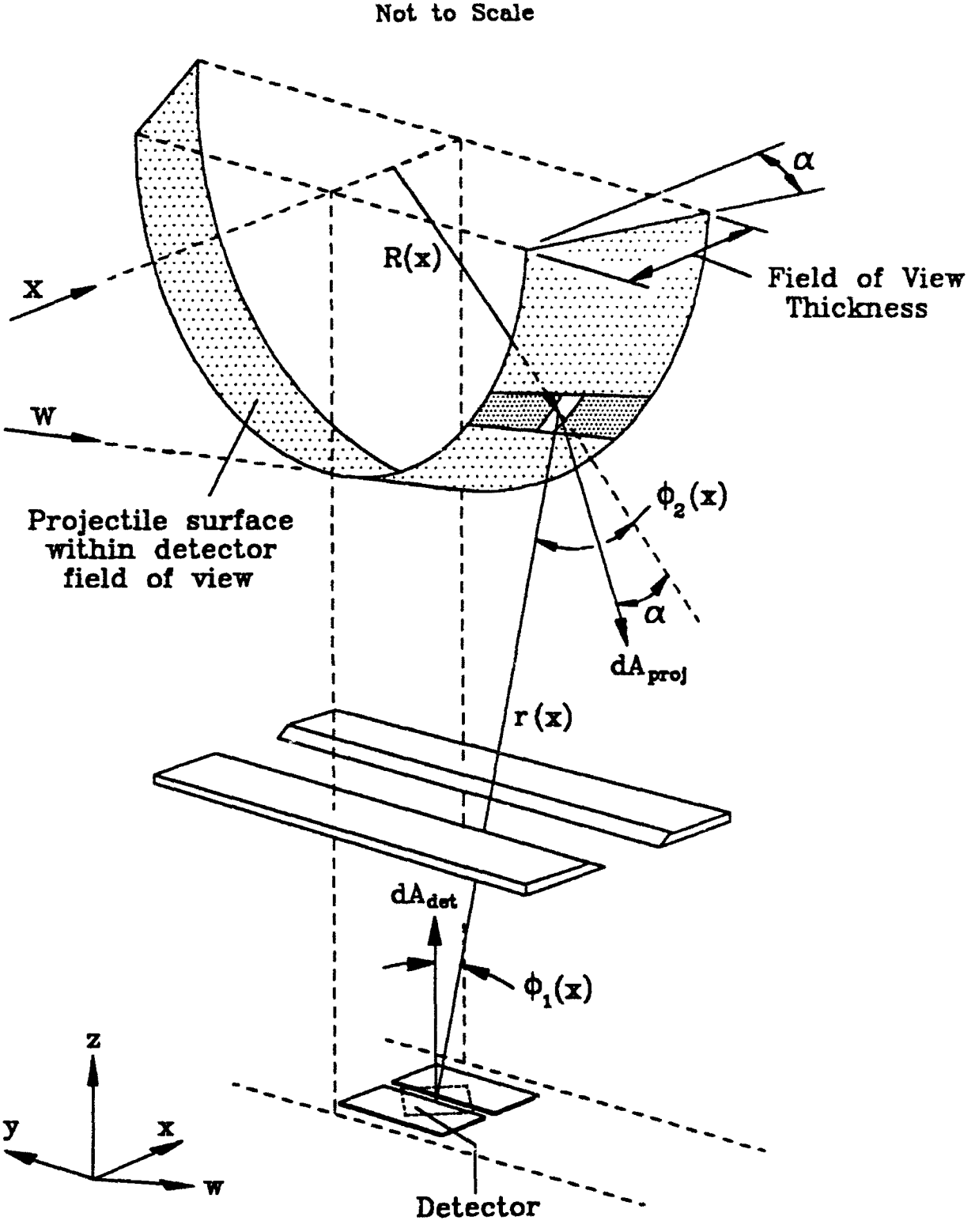

Figure 8. Experimental Configuration for a Portion of Projectile Nosecone

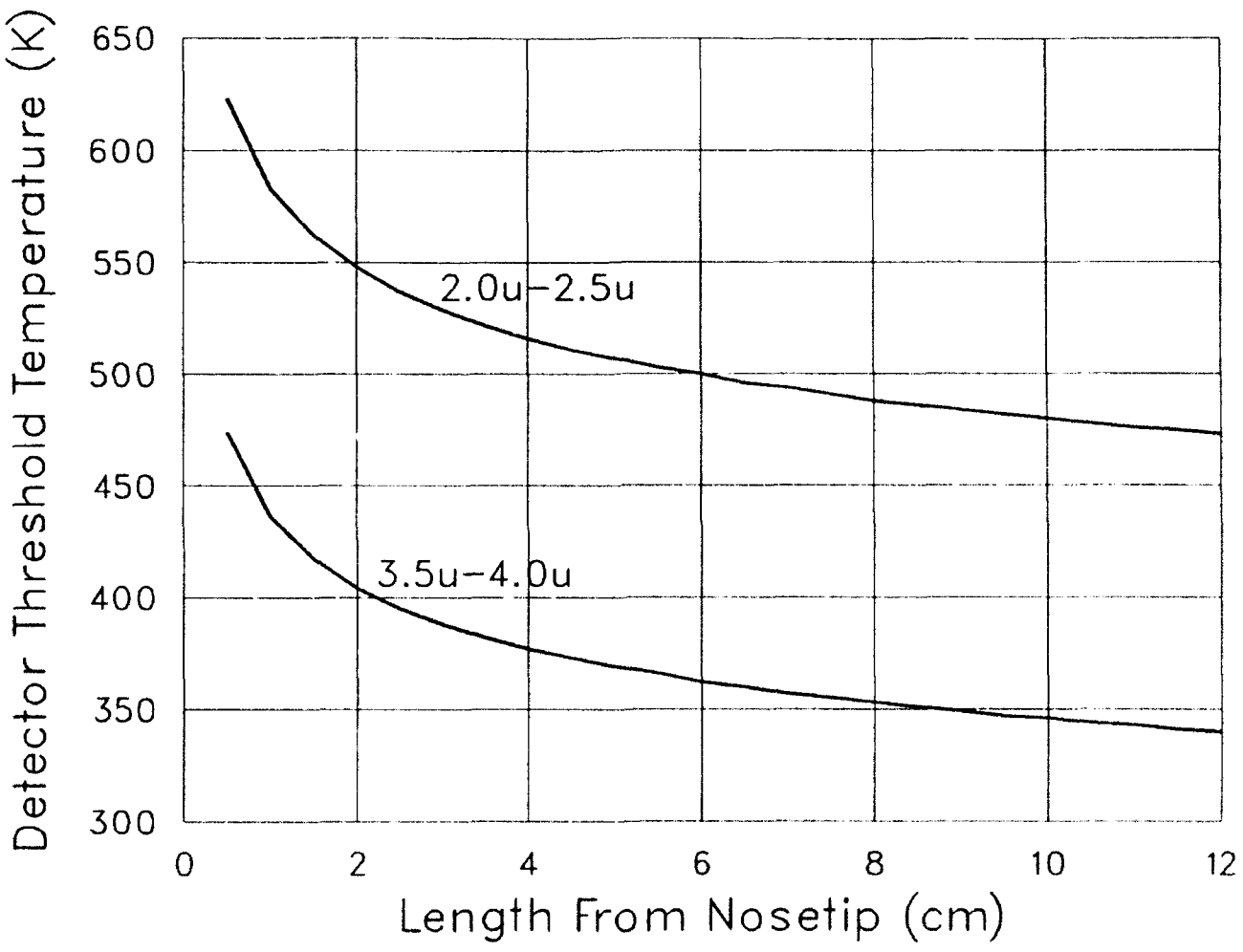

Figure 9. Detector Threshold Temperature Distribution

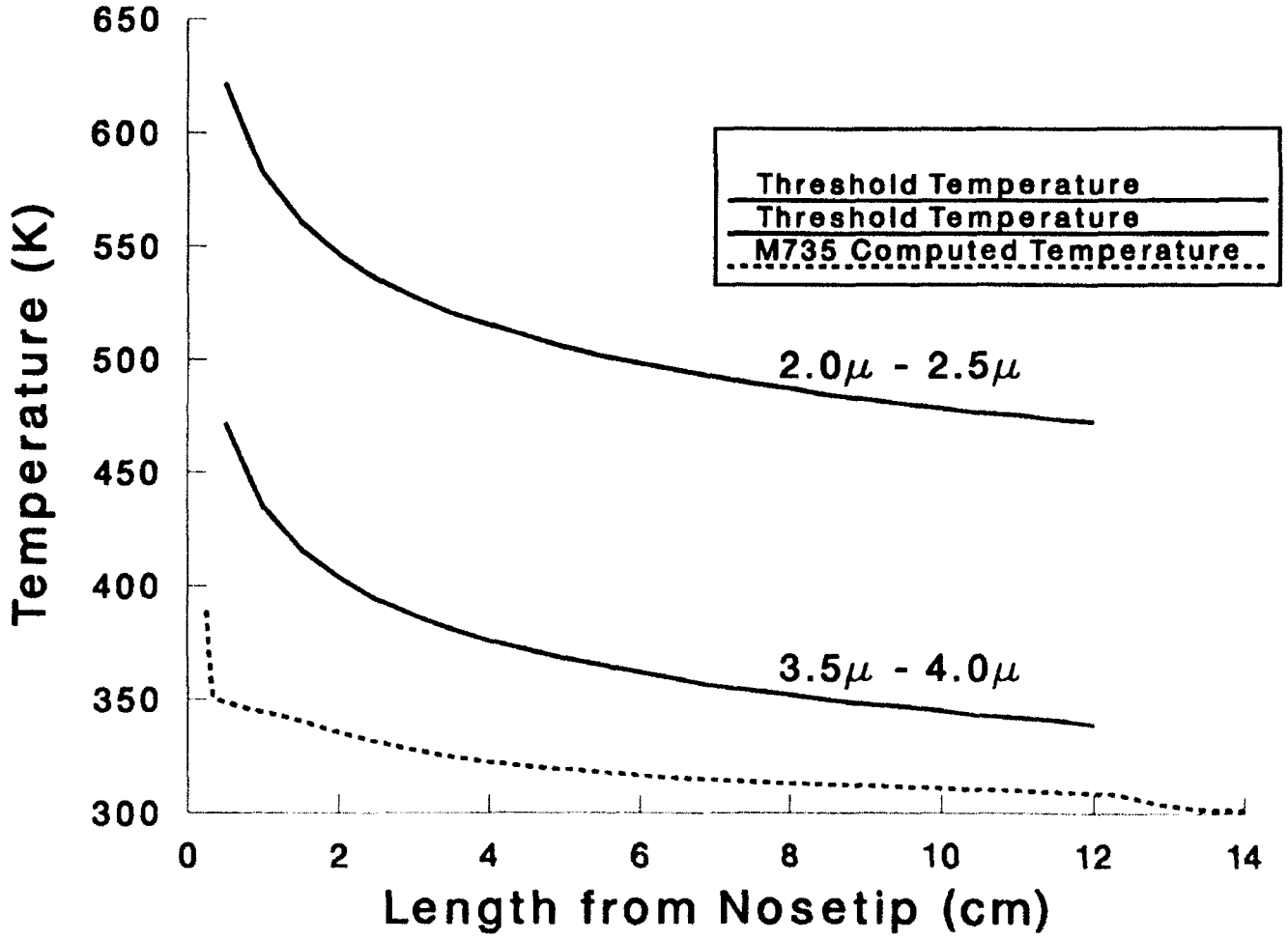

Figure 10. Detector Threshold vs. Computed Surface Temperature, M735, Range=225 m, Laminar Flow

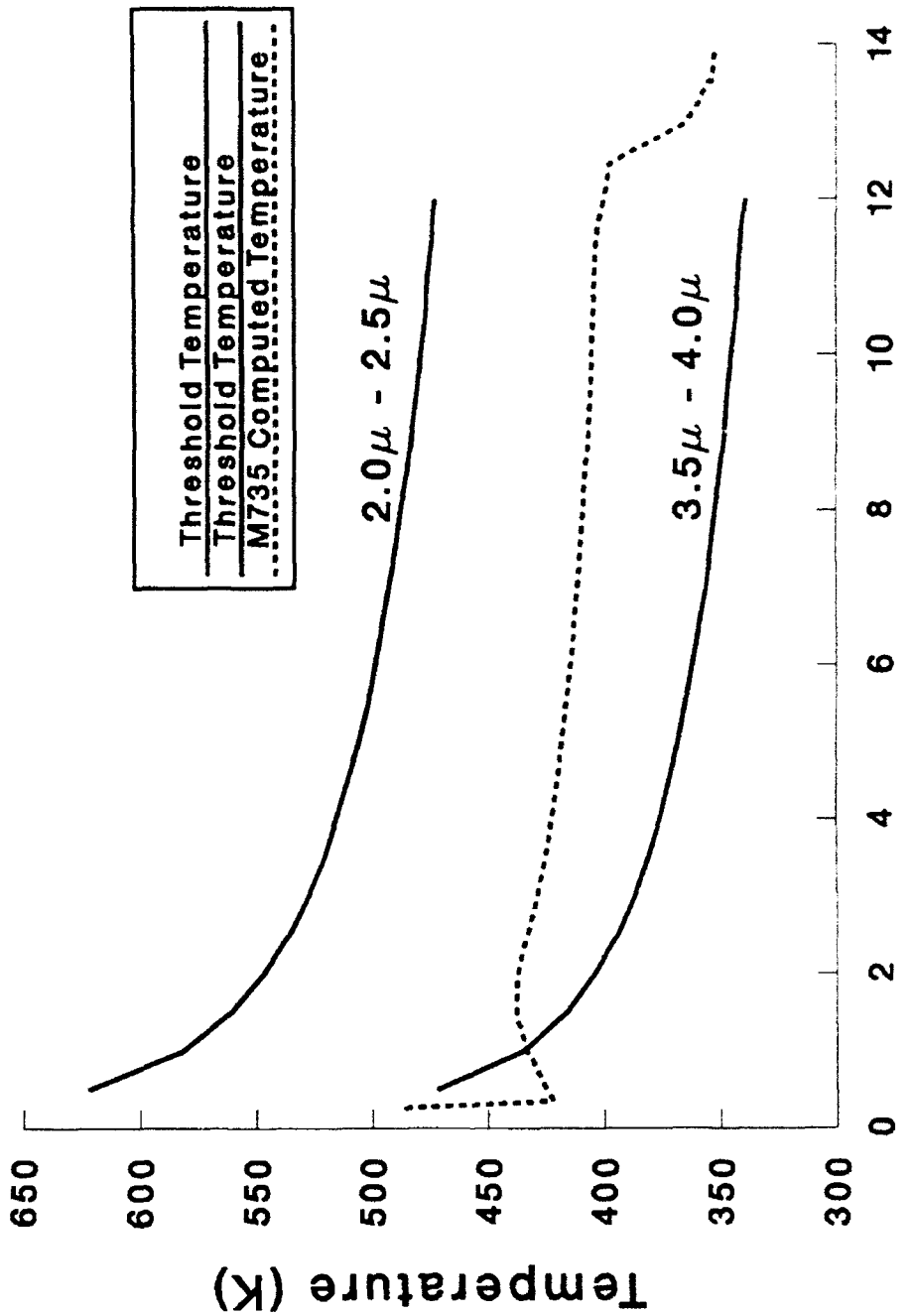

Figure 11. Detector Threshold vs. Computed Surface Temperature, M735, Range=225 m, Turbulent Flow

Table 1. Calculation of Detector Threshold Power

	Wavelength Sensitivity Band	
	$2.0\mu - 2.5\mu$	$3.5\mu - 4.0\mu$
Average Responsivity, A/W	1.75	2.65
Noise, $W/\sqrt{Hz}$	$17\text{x}10^{-12}$	$17\text{x}10^{-12}$
Average NEP, W	$9.71\text{x}10^{-12}$	$6.42\text{x}10^{-12}$
Equipment Noise Bandwidth, Hz	$1.0\text{x}10^{6}$	$1.0\text{x}10^{6}$
Safety Factor	10	10
Detector Threshold Power, W	$9.71\text{x}10^{-8}$	$6.42\text{x}10^{-8}$

Table 2. Detector Pertinent Data

Manufacturer	EG and G Judson
Model	J10D-M920-S05M-60
Type	Photovoltaic Indium-Animonide
Size	5 mm square
Peak Responsivity	3.892 A/W
Noise	$17x10^{-12}A/\sqrt{Hz}$

Table 3. Assumed constants

Nosecone Angle, α, deg	8.0
Projectile Radius, R, cm	1.77
Detector Diagonal, L, cm	0.71
Height of Projectile Above Detector, h, cm	100.0
Distance Off Center, y, cm	20.0
Field of View Half Angle, β, deg	0.286

INTENTIONALLY LEFT BLANK.

5. REFERENCES

1. Thomson, G. Private conversation. January-July 92.

2. Lowe, D.S. "Measurement of Surface Temperatures of a Projectile in Flight by Means of its Infrared Radiation." NAVORD-2145, July 1951.

3. Holman, J.P. Heat Transfer. McGraw-Hill, NY, NY, 1986.

4. Dereniak, E.L., and D.G. Crowe. Optical Radiation Detectors . John Wiley and Sons, NY, NY, 1984.

5. O'Leary, B., E.G. and G. Judson. Private conversation. May-July 1992.

6. Wolf, S. Guide to Electronic Measurements and Laboratory Practice. Prentice Hall, Inc., Englewood, NJ, 1983.

7. Hudson, R.D. Infrared System Engineering. John Wiley and Sons, N.Y., N.Y., 1969.

8. Wolfe, W. and G. Zissis. Infrared Handbook. Infrared Information Analysis Center, Revised Edition, 1989.

9. Gerald, C. Applied Numerical Analysis. Addison-Wesley Co., Reading, MA, 1978.

10. Guidos, B. "Computational Fluid Dynamics Prediction of M735 Projectile Forebody Temperature at Short Range." U.S. Army Research Laboratory, Aberdeen Proving Ground, MD 21005. (report to be published).

INTENTIONALLY LEFT BLANK.

No. of Copies	Organization
2	Administrator Defense Technical Info Center ATTN: DTIC-DDA Cameron Station Alexandria, VA 22304-6145
1	Commander U.S. Army Materiel Command ATTN: AMCAM 5001 Eisenhower Ave. Alexandria, VA 22333-0001
1	Director U.S. Army Research Laboratory ATTN: AMSRL-OP-CI-AD, Tech Publishing 2800 Powder Mill Rd. Adelphi, MD 20783-1145
1	Director U.S. Army Research Laboratory ATTN: AMSRL-OP-CI-AD, Records Management 2800 Powder Mill Rd. Adelphi, MD 20783-1145
2	Commander U.S. Army Armament Research, Development, and Engineering Center ATTN: SMCAR-IMI-I Picatinny Arsenal, NJ 07806-5000
2	Commander U.S. Army Armament Research, Development, and Engineering Center ATTN: SMCAR-TDC Picatinny Arsenal, NJ 07806-5000
1	Director Benet Weapons Laboratory U.S. Army Armament Research, Development, and Engineering Center ATTN: SMCAR-CCB-TL Watervliet, NY 12189-4050
(Unclass. only) 1	Commander U.S. Army Rock Island Arsenal ATTN: SMCRI-IMC-RT/Technical Library Rock Island, IL 61299-5000
1	Director U.S. Army Aviation Research and Technology Activity ATTN: SAVRT-R (Library) M/S 219-3 Ames Research Center Moffett Field, CA 94035-1000

No. of Copies	Organization
1	Commander U.S. Army Missile Command ATTN: AMSMI-RD-CS-R (DOC) Redstone Arsenal, AL 35898-5010
1	Commander U.S. Army Tank-Automotive Command ATTN: ASQNC-TAC-DIT (Technical Information Center) Warren, MI 48397-5000
1	Director U.S. Army TRADOC Analysis Command ATTN: ATRC-WSR White Sands Missile Range, NM 88002-5502
1	Commandant U.S. Army Field Artillery School ATTN: ATSF-CSI Ft. Sill, OK 73503-5000
(Class. only) 1	Commandant U.S. Army Infantry School ATTN: ATSH-CD (Security Mgr.) Fort Benning, GA 31905-5660
(Unclass. only) 1	Commandant U.S. Army Infantry School ATTN: ATSH-CD-CSO-OR Fort Benning, GA 31905-5660
1	WL/MNOI Eglin AFB, FL 32542-5000
	Aberdeen Proving Ground
2	Dir, USAMSAA ATTN: AMXSY-D AMXSY-MP, H. Cohen
1	Cdr, USATECOM ATTN: AMSTE-TC
1	Dir, ERDEC ATTN: SCBRD-RT
1	Cdr, CBDA ATTN: AMSCB-CI
1	Dir, USARL ATTN: AMSRL-SL-I
10	Dir, USARL ATTN: AMSRL-OP-CI-B (Tech Lib)

INTENTIONALLY LEFT BLANK.

USER EVALUATION SHEET/CHANGE OF ADDRESS

This Laboratory undertakes a continuing effort to improve the quality of the reports it publishes. Your comments/answers to the items/questions below will aid us in our efforts.

1. ARL Report Number ARL-MR-62 Date of Report April 1993

2. Date Report Received _____

3. Does this report satisfy a need? (Comment on purpose, related project, or other area of interest for which the report will be used.) _____

4. Specifically, how is the report being used? (Information source, design data, procedure, source of ideas, etc.) _____

5. Has the information in this report led to any quantitative savings as far as man-hours or dollars saved, operating costs avoided, or efficiencies achieved, etc? If so, please elaborate. _____

6. General Comments. What do you think should be changed to improve future reports? (Indicate changes to organization, technical content, format, etc.) _____

CURRENT ADDRESS

_____
Organization

_____
Name

_____
Street or P.O. Box No.

_____
City, State, Zip Code

7. If indicating a Change of Address or Address Correction, please provide the Current or Correct address above and the Old or Incorrect address below.

OLD ADDRESS

_____
Organization

_____
Name

_____
Street or P.O. Box No.

_____
City, State, Zip Code

(Remove this sheet, fold as indicated, tape closed, and mail.)
(DO NOT STAPLE)

DEPARTMENT OF THE ARMY

OFFICIAL BUSINESS

BUSINESS REPLY MAIL
FIRST CLASS PERMIT No 0001, APG, MD

Postage will be paid by addressee

Director
U.S. Army Research Laboratory
ATTN: AMSRL-OP-CI-B (Tech Lib)
Aberdeen Proving Ground, MD 21005-5066

NO POSTAGE
NECESSARY
IF MAILED
IN THE
UNITED STATES